sible reduction in reaction dimensionality.[11] Moreover, the ability to replace the more common octahedral lattice cations, Al(III) and Mg(II), with transition-metal cations suggests that new active sites can be generated.

Further tuning of the surface properties of such systems is possible by the implementation of other approaches. Certain transition-metal cations may be substituted for Si(IV) in the tetrahedral sheet in addition to or instead of substitutions in the octahedral sheet. Coordinatively unsaturated sites in the tetrahedral sheet should have even stronger Lewis acid strength than coordinatively unsaturated sites in the octahedral sheet because the lower the coordination number the greater should be the Lewis acidity. An example is the mineral sauconite[33] with the ideal chemical formula $(Zn_6)Si_{8-x}Zn_xO_{10}(OH)_2$. It may also be possible to gain some synthetic control over the particle size and hence the proportion of edge surface sites available. Finally, the exchange capacity of such transition-metal-substituted smectite clays can be exploited for more traditional modification of surface properties.

Conclusions

Fluorohectorite clay was synthesized in which Cu(II) is substituted for Mg(II) in the octahedral sheet. These results provide reasonably definitive evidence for this substitution which has also been suggested for the related mineral stevensonite.[10,34] Copper(II) does not seem to preferentially occupy one type of site with respect to Li(I) substitution. We have also demonstrated that total substitution of Cu(II) for Mg(II) can be achieved.

A consequence of Cu(II) for Mg(II) substitution is that some of the Cu(II) exists at edge lattice sites of the fluorohectorite crystals. These are coordinatively unsaturated and are capable of binding Lewis base adsorbate molecules, apparently with some degree of selectivity. The substitution of one or a combination of transition-metal ions in different lattice sites may represent a means of tailoring smectite surface acidity for specific catalytic applications.

Acknowledgment. This work was supported by the Robert A. Welch Foundation, the Texas Advanced Research Program, and the National Science Foundation.

Registry No. NH_3, 7664-41-7; H_2O, 7732-18-5; C_6H_6, 71-43-2; Cu^{2+}, 15158-11-9; $Na_{0.5}(Mg_{2.49}Cu_{0.01}Li_{0.5})Si_4O_{10}F_2$, 136952-82-4; $Na_{0.5}(Mg_{2.25}Cu_{0.25}Li_{0.5})Si_4O_{10}F_2$, 136952-81-3; $Na_{0.5}(Cu_{2.5}Li_{0.5})Si_4O_{10}(OH)_2$, 136952-80-2; pyridine, 110-86-1; hectorite, 12173-47-6.

(33) Donor, H. E.; Mortland, M. M. *Science* **1981**, *166*, 1406.

(34) McBride, M. B. *Clays Clay Miner.* **1976**, *24*, 211.

Infrared Studies of CO Adsorption on Rhodium Hydrosols

M. R. Mucalo and R. P. Cooney*

Chemistry Department, University of Auckland, Private Bag, Auckland, New Zealand

Received May 24, 1991. Revised Manuscript Received August 26, 1991

Infrared spectra of CO adsorbed on poly(vinyl alcohol)-protected rhodium hydrosols exhibit two bands in the regions 2030–2040 and 1890–1900 cm^{-1}, which have been assigned respectively to CO adsorbed on linear and 2-fold-bridging rhodium metal surface sites. The band positions for adsorbed CO species on rhodium resemble those observed in infrared spectra of CO adsorbed on polycrystalline rhodium electrodes. When the pH was adjusted above the natural hydrosol pH of ca. 2.2, $\nu(CO)_{ads}$ was observed to decrease. This was attributed to the lower CO coverage resulting from hydroxyl adsorption and to surface oxide formation on the rhodium particles. Values of $d\nu/d\psi_0$ derived from $d\nu/d(pH)$ values for CO adsorbed on rhodium hydrosol particles (pH < ca. 2.2) were in the range 26–40 cm^{-1} V^{-1}. These were similar to values reported from in situ spectroelectrochemical studies of CO adsorbed on polycrystalline rhodium electrodes (40 cm^{-1} V^{-1}) and of CO adsorbed on single-crystal rhodium electrodes (35 cm^{-1} V^{-1}) in acidic media, thus indicating similarities between adsorption on electrode and colloid surfaces. X-ray photoelectron spectra of rhodium flocs prepared in the absence of poly(vinyl alcohol) revealed the presence of surface Rh_2O_3 and residual $RhCl_3$.

Introduction

Previous work has centered on characterizing CO adsorbed on platinum and palladium colloids in various dispersion media. For example, infrared spectra of CO adsorbed on colloidal platinum in CH_2Cl_2 have revealed[1] bands due to linearly adsorbed CO (2050 cm^{-1}) and 2-fold-bridged (B_2) CO (1880 cm^{-1}). Bands assigned to linear (2062 cm^{-1}) and 2-fold-bridge adsorbed CO (1941 cm^{-1}) were also detected[2] in infrared studies of CO adsorbed on palladium colloids in methylcyclohexane media. Infrared spectra of CO adsorbed on aqueous platinum colloids (hydrosols) feature[3] a band at 2065–2070 cm^{-1} due to CO adsorbed linearly on platinum while spectra of CO adsorbed[4] on palladium hydrosols reveal 2-fold bridged CO species (ca. 1950 cm^{-1}) in addition to linearly adsorbed CO species (ca. 2067 cm^{-1}). The band due to CO adsorbed linearly on platinum (ca. 2070 cm^{-1}) has been used in recent studies of surface processes in platinum hydrosols. The effect of electrolytes,[5] aliphatic alcohols,[6] and pH

(1) Lewis, L. N.; Lewis, N. *J. Am. Chem. Soc.* **1986**, *108*, 7228.

(2) Bradley, J. S.; Millar, J.; Hill, E. W.; Melchior, M. *J. Chem. Soc., Chem. Commun.* **1990**, 705.

(3) Mucalo, M. R.; Cooney, R. P. *J. Chem. Soc., Chem. Commun.* **1989**, 94.

(4) Mucalo, M. R.; Cooney, R. P. *J. Chem. Soc., Faraday Trans.* **1991**, *87*, 1221.

(5) Mucalo, M. R.; Cooney, R. P. *Can J. Chem.* (R. N. Jones Special Issue), to appear November, 1991.

(6) Mucalo, M. R.; Cooney, R. P., submitted to *J. Chem. Soc., Faraday Trans.*, in press.

0897-4756/91/2803-1081$02.50/0

adjustment[4] on the surface speciation and adsorption properties of platinum hydrosols (as reflected by changes in $\nu(CO)_{ads}$) has been reported.

Colloidal rhodium has been used in conjunction with $([Ru(bipy)_3^{2+}]/H_2dmbipy^{2+}$ (1,1'-dimethyl-4,4'-bipyridinium, as the dichloride salt) and disodium EDTA (ethylenediaminetetraacetate) for the photoproduction of hydrogen[7] from water. In such systems, the rhodium colloid has been of value as a hydrogenation catalyst for the reduction of organic compounds containing C=C and C≡C bonds.[7] Finely divided rhodium metal incorporated into car exhaust catalyst systems has been found[8] to provide additional oxygen storage capacity via chemisorption of oxygen at lower operating temperatures. Infrared studies of CO adsorption on rhodium are well-documented for single-crystal, electrode, thin metal film and supported metal catalyst surfaces.[9-16] In situ infrared spectra of CO adsorbed on colloidal rhodium have yet to be reported. Infrared spectra of CO adsorbed on alumina-supported rhodium metal catalysts have commonly featured[9-12] a pair of bands at ca. 2100 and ca. 2030 cm^{-1}, which have been assigned to a surface rhodium *gem*-dicarbonyl complex. It has also been proposed[9] that the 2100-cm^{-1} band may be due to CO adsorbed on incompletely reduced rhodium sites. Additional bands in the regions 2040–2060 and 1900–1925 cm^{-1} have also been detected[10] on alumina-supported rhodium, which have been assigned respectively to linearly adsorbed and 2-fold-bridge-adsorbed CO on rhodium metal surface sites. CO adsorption on polycrystalline rhodium electrodes in neutral and acidic solution is characterized[13,14] by the appearance of two bands in infrared spectra at ca. 2030 and 1890–1900 cm^{-1} which have been assigned respectively to linearly adsorbed and 2-fold-bridge-adsorbed (B_2) CO on rhodium metal. In one study,[15] infrared spectra of CO adsorption on rhodium electrodes partially coated with copper adatoms by under-potential deposition (UPD) showed that the B_2 mode of adsorbed CO was significantly retarded in the presence of copper. In situ infrared spectra of CO adsorption on ordered and disordered single-crystal (Rh(111)) electrodes also reveal[14] two bands in the wavenumber regions 2020–2040 and 1790–1910 cm^{-1}, which have been assigned respectively to linear and bridged CO species. Broader $\nu(CO)_{ads}$ bands are observed for CO adsorbed on disordered Rh(111) single crystals. In addition, significantly higher $\nu(CO)_{ads}$ values (1890–1910 cm^{-1}) for bridged carbonyls are observed. Indeed, the frequency of bridged CO species on disordered rhodium single crystals is similar to the corresponding band observed for CO adsorbed on polycrystalline rhodium in acidic media (see earlier). Oxidation–reduction cycles of rhodium electrodes during CO bubbling[16] were found to lead to the formation of carbonyl rhodium cluster compounds on the electrode surface which gave intense potential-independent bands at 2080 and 1810 cm^{-1}. The surface cluster compounds were believed to form in the reaction of freshly formed rhodium clusters with dissolved CO.

In the present study, surface processes occurring on rhodium hydrosols studied by Fourier transform infrared spectroscopy using CO as a spectroscopic probe will be described. The behavior of CO adsorbed on rhodium hydrosols will be compared with that of CO adsorbed at rhodium electrodes. Determination of particle shape and particle size distributions by transmission electron microscopy will also be discussed. In addition, surface speciation on unprotected rhodium hydrosol flocs as revealed by X-ray photoelectron spectroscopy will be considered.

Experimental Section

Reagents. The rhodium trichloride used to prepare rhodium hydrosols was supplied by Engelhard Chemicals as $RhCl_3 \cdot xH_2O$ and contained 40.91% Rh. The sodium borohydride (general purpose reagent) and perchloric acid (analytical grade) were supplied by BDH Chemicals. The poly(vinyl alcohol) used in preparations was BDH laboratory grade reagent, which was estimated to have an average molecular weight of 2.7×10^4 g mol^{-1} as determined by viscosity measurements. Potassium hydroxide was provided in pelletized form by Scientific Supplies Ltd, Auckland. These reagents were used without further purification. Millipore water obtained by passing singly distilled water through a Milli-Q Continental Water System was used in the preparation of solutions and hydrosols.

Preparation and Characterization of Rhodium Hydrosols. Rhodium hydrosols were prepared by borohydride reduction of rhodium trichloride solutions in the presence of poly(vinyl alcohol), which acted as a protecting agent. Rhodium hydrosols prepared in the absence of poly(vinyl alcohol) tended to aggregate almost immediately after formation, forming thick black flocs. Two methods of preparation were used. In the first method (method A), 6.0 mL of ca. 0.03 M $RhCl_3$ solution was mixed with 15 mL of water and 5 mL of ca. 3.1% (w/w) poly(vinyl alcohol) solution and cooled to ca. 2 °C. Then 9.75 mL of ca. 0.03 M cool, freshly prepared sodium borohydride was added dropwise to the stirred $RhCl_3$ solution, which turned the initially dark orange solution to a jet-black color accompanied by foaming of the reaction solution associated probably with hydrogen evolution during the reduction. The hydrosol was subsequently subjected to ion-exchange for 10–20 min using Amberlite MB1 cation–anion ion-exchange resin. Ion-exchange of PVA-protected hydrosols caused a decrease in the initial conductivity of 2000–4000 μS cm^{-1} to values of 12–17 μS cm^{-1} after which further ion exchange led to no additional decrease in conductivity. In the second method (method B), 9.75 mL of ca. 0.07 M cool, freshly prepared sodium borohydride was added dropwise to a stirred solution of 10 mL of ca. 0.03 M $RhCl_3$ and 1–1.5 mL of ca. 3.1% (w/w) poly(vinyl alcohol) solution at 3 °C. The resultant jet-black hydrosol was then used in experiments without ion exchange. The natural pH of this sol was ca. 2.2. This value refers to the pH of the hydrosol directly after preparation or in the case of ion-exchanged hydrosols directly after ion-exchange. An unprotected borohydride-generated rhodium hydrosol prepared specifically for surface analysis by X-ray photoelectron spectroscopy was obtained by adding 9.75 mL of cool freshly prepared (ca. 0.045 M) sodium borohydride to a cooled (0–5 °C) solution of 9.0 mL of 0.03 M $RhCl_3$ and 1.0 mL of water. The clear reaction solution was decanted from the resulting large black flocs of rhodium metal. The flocs were subsequently washed four times with a solution (ca. 0.02 M perchloric acid) which was of similar pH to the original reaction solution. Turbidity measurements of both method A and method B borohydride-generated rhodium hydrosols were taken at 450 nm in ultraviolet/visible spectra of 5–10-fold diluted hydrosols as was done in earlier studies[4] of platinum and palladium hydrosols. Turbidity is an indirect measure of particle concentration in the hydrosol.

Transmission Electron Microscopy. In general, the method A (ion-exchanged) rhodium hydrosol was used in TEM studies

(7) Tan, C.-K.; Newberry, V.; Webb, T. R.; McAuliffe, C. A. *J. Chem. Soc., Dalton Trans.* **1987**, 1299.
(8) Lööf, P.; Kasemo, B.; Keck, K. E. *J. Catal.* **1989**, *118*, 339.
(9) Sheppard, N.; Nguyen, T. T. *Advances in Infrared and Raman Spectroscopy*; Clark, R. J. H., Hester, R. E., Eds.; Wiley-Heyden: London, 1978; Vol. 5, p 106.
(10) Yang, A. C.; Garland, C. W. *J. Phys. Chem.* **1957**, *61*, 1504.
(11) Anderson, J. A.; Millar, G. J.; Rochester, C. H. *J. Chem. Soc., Faraday Trans.* **1990**, *86*, 571.
(12) Unland, M. L. *J. Catal.* **1973**, *31*, 459.
(13) Kunimatsu, K.; Lezna, R. O.; Enyo, M. *J. Electroanal. Chem.* **1989**, *258*, 115.
(14) Leung, L.-W. H.; Chang, S.-C.; Weaver, M. J. *J. Chem. Phys.* **1989**, *90*, 7426.
(15) Beden, B.; Bewick, A.; Kunimatsu, K.; Lamy, C. *J. Electroanl. Chem.* **1982**, *142*, 345.
(16) Ikezawa, Y.; Yoshii, S.; Takamura, T. *J. Electroanal. Chem.* **1991**, *301*, 241.

to avoid micrographs featuring particles trapped in salts co-deposited with the rhodium particles. The unprotected (aggregated) rhodium hydrosol prepared specifically for analysis by X-ray photoelectron spectroscopy was not examined by TEM because the flocs produced were too thick to be deposited and satisfactorily examined under the transmission electron microscope. Micrographs were acquired of rhodium hydrosol particles deposited onto collodion 40-mesh graphitic copper grids. Particle size measurements were carried out using an image-processing program called V (Digital Optics Ltd) which employed a Matrox PIP 512 image-grabbing board and Sony camera.

X-ray Photoelectron Spectroscopy. X-ray photoelectron spectra of the flocs produced in the preparation of the unprotected rhodium hydrosol were recorded using a Kratos XSAM 800 X-ray photoelectron spectrometer using a DS800 data system. Wide scans (0–800 eV) using nonmonochromatized Mg Kα radiation were obtained of the rhodium samples dry-deposited onto stainless steel stubs. Evaporation of the aqueous (perchloric acid) medium from the washed flocculated rhodium particles was carried out in situ in the preparation chamber of the Kratos XSAM. Narrow scans using nonmonochromatized Mg Kα radiation with an electron pass energy of 20 eV were subsequently obtained over the Rh(3d) (300–320 eV)) and C(1s) (280–290 eV) energy windows. The binding energy position[17] of C(1s) (284.8 eV) which was assumed to arise predominantly from adventitious hydrocarbons was used as an internal reference in most X-ray photoelectron spectra. Sputtering of the rhodium samples, carried out using a 3-kV argon ion gun, was normally conducted for periods of 10–20 min. 90% Gaussian/10% Lorentzian spin–orbit doublets[4] were fitted to Rh(3d) XPS profiles obtained in narrow scans using conventional curve-fitting routines supplied by the DS800 software. A minimum of three spin-orbit doublets each constrained to have an area ratio of 1.5:1 (given by the ratio of the respective degeneracies for the Rh(3d) peak) and a spin–orbit coupling constant of 4.70 eV[18] were fitted to the experimental Rh(3d) XPS profile.

Infrared Spectroscopy. All infrared spectra were acquired at 4-cm^{-1} resolution using a Digilab FTS-60 Fourier transform infrared spectrometer as described in earlier studies.[4-6] Samples for infrared analysis were prepared by treating ca. 0.15 mL of rhodium hydrosol with CO gas for 10 min. Spectra were recorded (20 scans) of the hydrosol held as a thin film between calcium fluoride windows without spacers. Spectral acquisition times were of the order of 20 s. Spectra of water or untreated rhodium hydrosols were then subtracted from the spectrum of the CO-treated rhodium hydrosol in order to reveal the bands due to $\nu(CO)_{ads}$. The method B rhodium hydrosol was used mostly in infrared studies because of its greater surface area. Ion exchange of rhodium hydrosols was found to lead to a significant loss of particles possibly by adsorption[19] on the ion-exchange resin. This loss resulted in a hydrosol of lower surface area which consequently led to the observation of weaker bands due to $\nu(CO)_{ads}$. CO adsorption on the rhodium hydrosols as a function of pH was also studied. The pH values of the hydrosol samples were altered to the selected values by potassium hydroxide or perchloric acid addition followed by CO treatment for 10 min. CO coverage was assessed from the calculation of normalized[4] absorbance ($A'(CO)$) values. In general terms, this involved the normalization of observed $\nu(CO)_{ads}$ band intensity with respect to the turbidity of the rhodium hydrosol measured at 450 nm (see earlier).

Results and Discussion

(i) Transmission Electron Microscopy. Figure 1a illustrates the transmission electron micrograph of an ion-exchanged PVA-protected rhodium hydrosol. Clustering of approximately spherical particles was a typical characteristic of rhodium hydrosol micrographs. Indeed, Lewis et al.[20] observed significant particle–particle interaction in high-resolution electron micrographs (HREM)

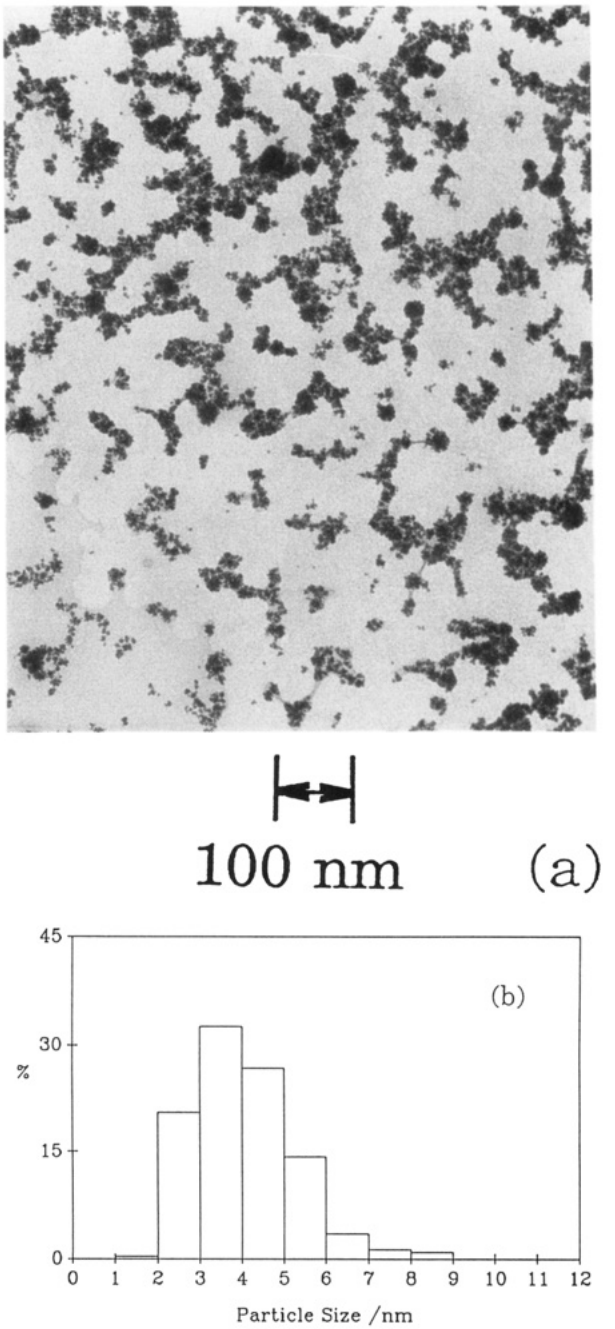

Figure 1. (a) Transmission electron micrograph and (b) particle size distribution of a PVA-protected borohydride-generated rhodium hydrosol.

of rhodium colloids prepared by reduction of $RhCl_3$ in $Me_2(EtO)SiH$. In contrast, transmission electron micrographs of the unprotected platinum and palladium hydrosols generated by borohydride reduction usually exhibited[21] approximately spherical particles linked together to form necklace-like patterns (i.e., necklacing) which was assumed to arise from partial sintering of the particles by H_2 during the preparation of the hydrosols. However, there was a general absence of particle necklacing in transmission electron micrographs of PVA-protected platinum hydrosols.[6] Figure 1b illustrates the particle size distribution for the PVA-protected rhodium hydrosol. The average particle diameter of the hydrosol was found to be ca. 4.0 nm with a dispersion of particles over a wide range from 1.0 to 9.0 nm (see Figure 1b).

(17) Carlson, T. A. *Photoelectron and Auger Spectroscopy*; Plenum Press: New York, 1975; p 364.
(18) Mårtennsson, N.; Nyholm, R. *Phys. Rev. B* **1981**, *24*, 7121.
(19) Nakao, Y.; Kaeriyama, K. *J. Colloid Interface Sci.* **1989**, *131*, 186.
(20) Lewis, L. N.; Lewis, N. *Chem. Mater.* **1989**, *1*, 106.
(21) Mucalo, M. R.; Cooney, R. P.; Metson, J. B. *Colloids Surf.*, in press.

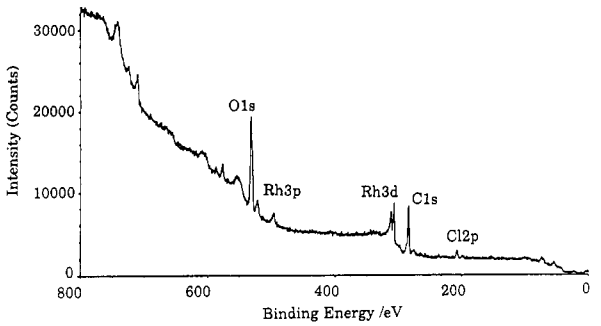

Figure 2. Wide X-ray photoelectron spectrum of an unprotected rhodium hydrosol.

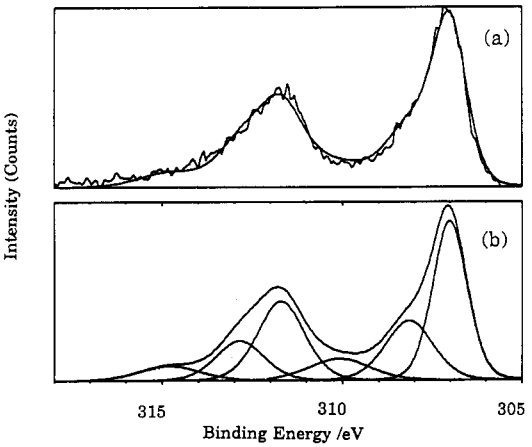

Figure 3. Narrow-scan X-ray photoelectron spectrum together with curve-fit analysis over the Rh(3d) region for an unprotected rhodium hydrosol: (a) resultant curve-fitted Rh(3d) XPS profile superimposed on the experimental Rh(3d) XPS profile and (b) the component spin-orbit doublets comprising the resultant curve-fitted Rh(3d) XPS profile.

(ii) X-ray Photoelectron Spectroscopy. Determination of rhodium surface speciation by X-ray photoelectron spectroscopy of the PVA-protected rhodium hydrosols was not feasible because the spectra were dominated by C(1s) and O(1s) peaks of the thick poly(vinyl alcohol) layer which coated the rhodium particles after evaporation of the aqueous sol media. XPS data were obtained of a rhodium colloid in the absence of poly(vinyl alcohol). A wide scan of the rhodium flocs from 0 to 800 eV is given in Figure 2. Peaks (C(1s) and O(1s)) arising mostly from adventitious hydrocarbon impurities and adsorbed water on the sample and holder[21] were detected. Weak Cl(2p) peaks at ca. 200 eV (residual $RhCl_3$) and 208.8 eV (residual perchlorate from the washing solution) were also observed. Previous workers have reported[22,23] that finely divided Rh prepared for catalytic purposes from borohydride reduction of aqueous solutions of the corresponding metal salts contains small quantities (ca. 2–3% boron) as borides. However, boron was not detected in X-ray photoelectron spectra of the rhodium flocs in this study (Figure 2). A narrow scan over the Rh(3d) region (305–318 eV) is shown in Figure 3. In general, it was noted that the $Rh(3d_{3/2})$ peak was significantly broader and less intense than expected from the ratio of relative degeneracies ($2S + 1$), than the $Rh(3d_{5/2})$ peak. The broadening is a result[18] of an $M_4M_5N_{45}$ Coster–Kronig decay channel which considerably reduces the lifetime of the $Rh(3d_{3/2})$ hole state. In

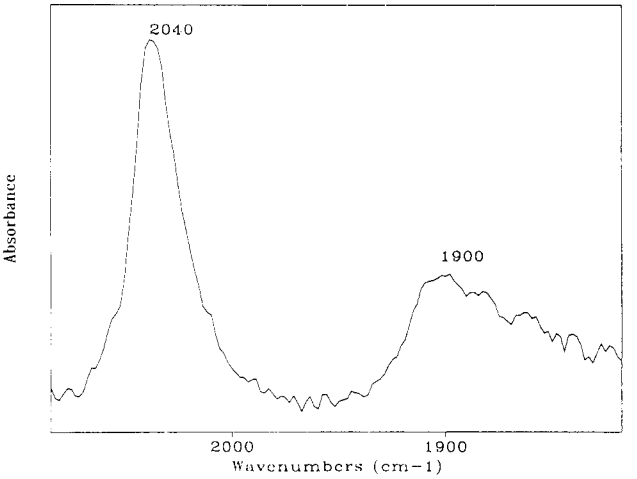

Figure 4. Typical infrared spectrum of CO adsorbed on a rhodium hydrosol. The rhodium hydrosol had not previously been subjected to ion exchange.

general, the $M_4M_4N_{45}$ Coster–Kronig process involves the $3d_{3/2}$ hole state decaying into a $3d_{5/2}$ hole and an additional 4d valence band hole. For Rh metal, the Coster–Kronig broadening is ca. 0.4 eV on top of the natural line width of the $Rh(3d_{3/2})$ peak.[18] In general, a minimum of three spin–orbit doublets could be curve-fitted to the Rh3d XPS profile (see Figure 3). The most intense curve-fitted doublet ($Rh(3d_{5/2})$ = 307.75 eV after correction for C(1s)) was due to rhodium metal. An acceptable fit could only be obtained by selectively broadening the $Rh(3d_{3/2})$ line of the spin–orbit doublet for rhodium metal by an amount[18] equal to the Coster–Kronig broadening (ca. 0.4 eV).

The second curve-fitted doublet at 308.89 eV was shifted 1.14 eV from the binding energy of rhodium metal. Previous XPS studies[24-27] of rhodium catalysts, electrodes, and foils have reported binding energy shifts of 1.1–1.6 eV from rhodium metal which have been commonly assigned to rhodium sesquioxide (Rh_2O_3). In the present study, it is, therefore, likely that this oxide species is present on the surfaces of the rhodium flocs.

The third curve-fitted doublet is shifted ca. 3.1 eV from the binding energy for the metal. Binding energy shifts of this magnitude have been assigned[17] to $RhCl_3$ (3.3–3.4 eV). Given that Cl(2p) is also detected in the wide scan of the rhodium sample (see above), it is possible that the third curve-fitted doublet could be assigned to residual $RhCl_3$. The doublet is not likely to be due to RhO_2 as this species is reported[27] to exhibit a binding energy shift of 1.85 eV from rhodium metal. Thus X-ray photoelectron spectra have demonstrated that Rh_2O_3 and $RhCl_3$ are present on the surfaces of the unprotected rhodium hydrosol particles. It is a reasonable assumption that such species also exist on the surfaces of rhodium hydrosols protected by poly(vinyl alcohol). Some support for this assumption may be obtained from earlier infrared studies of CO adsorption on platinum hydrosols in alcoholic media[6] where association of the OH group of the alcohol with surface hydroxyls on the platinum hydrosol was believed to cause inhibition of CO adsorption. In the presence of poly(vinyl alcohol), interaction[6] via unhydrolyzed carbonyl groups with the hydrosol oxide surface may be important

(22) Polovnikov, B. D.; Balandin, A. A.; Taber, A. M. *Dokl. Akad. Nauk SSSR* **1962**, *145*, 809.
(23) Taber, A. M.; Polonikov, B. D.; Mal'tseva, N. N.; Mikheeva, V. I.; Balandin, A. A. *Dokl. Akad. Nauk SSSR* **1963**, *152*, 119.
(24) Brinen, J. S.; Melera, A. *J. Phys. Chem.* **1972**, *76*, 2525.
(25) Brinen, J. S.; Schmitt, J. L.; Doughman, W. R.; Achorn, P. J.; Siegel, L. A. *J. Catal.* **1975**, *40*, 295.
(26) Barr, T. L. *J. Phys. Chem.* **1978**, *82*, 1801.
(27) Hall, H. Y.; Sherwood, P. M. A. *J. Chem. Soc., Faraday Trans. 1* **1984**, *80*, 2867.

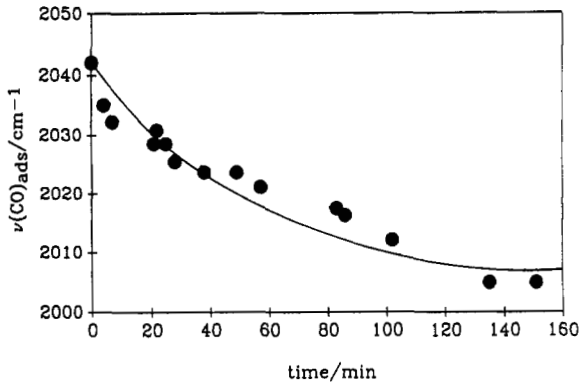

Figure 5. ν(CO)$_{ads}$ vs time after preparation of CO-treated sample for CO adsorbed on a rhodium hydrosol.

in the protection of the hydrosol. An earlier XPS study of borohydride-generated platinum hydrosols[21] concluded that a partial coverage of platinum(II) oxides were present on the surfaces of the colloid particles. Another study[5] relating to the effect of added electrolytes on CO adsorption on platinum hydrosols reported evidence for the reaction of I^- with a surface layer of platinum(II) oxide on the platinum hydrosol to form $[PtI_4]^{2-}$. The combination of in situ and ex situ results strongly suggests the existence of a partial oxide film in that related case.

(iii) Rh Sol/CO at Natural pH (ca. 2.2). Figure 4 is an infrared spectrum of a CO-treated rhodium hydrosol at natural pH (ca. 2.2) which had not been subjected to ion exchange. Infrared spectra of CO-treated rhodium hydrosols at natural pH usually exhibited two bands in the wavenumber regions 2030–2040 and 1890–1900 cm^{-1} which were assigned respectively to linearly adsorbed CO and 2-fold-bridge adsorbed (B_2) CO on rhodium metal surface sites (see Introduction). CO-treated rhodium hydrosols prepared with or without ion-exchange gave very similar infrared spectra.

The absence of a band at ca. 2100 cm^{-1} excluded the possibility that *gem*-dicarbonyl species could be responsible[9] for the band observed at 2030–2040 cm^{-1}. Thus it appears that the behavior of CO adsorbed on rhodium hydrosols is similar to that of CO adsorbed on polycrystalline rhodium electrodes and disordered Rh(111) single-crystal electrodes where bands due only to linear and bridged CO are observed.[13-15]

When a sample of CO-treated rhodium hydrosol is examined by infrared spectroscopy as a function of time after CO treatment, the ν(CO)$_{ads}$ band assigned to linearly adsorbed CO on rhodium is observed to shift to lower wavenumbers as is the case[3] for CO adsorbed linearly on platinum (ca. 2070 cm^{-1}). Figure 5 illustrates the decrease of ν(CO)$_{ads}$ with time. Initially, a relatively sharp decrease in ν(CO)$_{ads}$ is observed followed by a gradual leveling of the frequency at ca. 2000 cm^{-1} after 2 h of standing time. It is likely that desorption of CO from the rhodium surface is induced by warming by the infrared beam, thus leading to a decrease in CO coverage over time which is reflected in the overall decrease in absorbance of the ν(CO)$_{ads}$ band. Indeed, the promotion of CO desorption by the infrared beam has been demonstrated in the Pt sol/CO system where infrared spectra were recorded[28] of hydrosols with time (after CO treatment) from a CO-treated sample not kept in the infrared beam. This showed a decrease in ν(CO)$_{ads}$ from ca. 2065–2070 to 2060 cm^{-1} in 30 min of standing time as opposed to ca. 4 min[3] when the sample

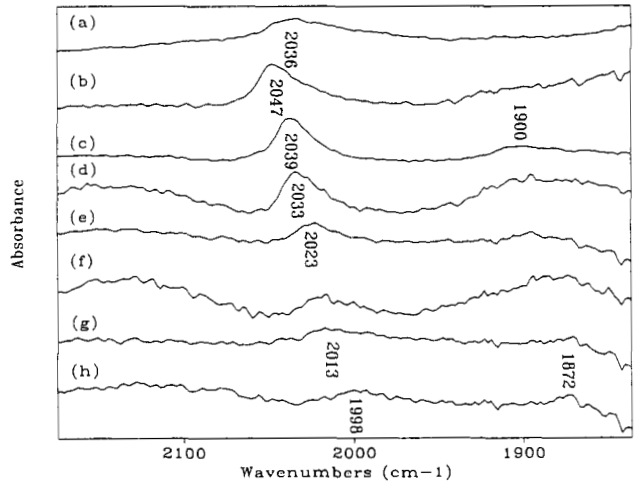

Figure 6. Series of infrared spectra of CO adsorbed on a rhodium hydrosol at pH: (a) 0.41, (b) 1.51, (c) natural pH (2.2), (d) 3.78, (e) 6.80, (f) 8.29, (g) 9.86, and (h) 11.35.

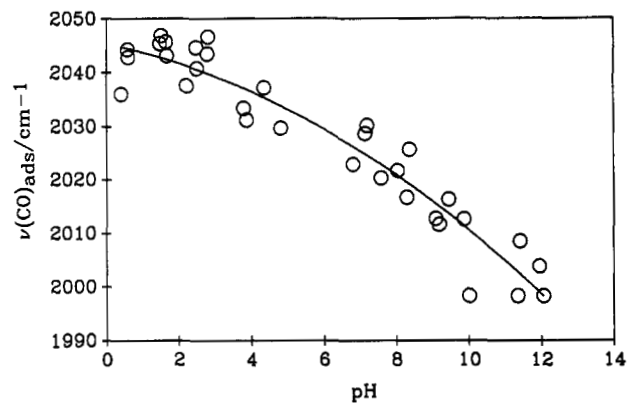

Figure 7. ν(CO)$_{ads}$ vs pH for the Rh sol/CO system. A polynomial of order x^2 has been fitted to the frequency–pH data.

is left in the infrared beam. Loss of dipole–dipole coupling between surface-adsorbed CO molecules[29] as CO coverage decreases is known to cause a decrease in ν(CO)$_{ads}$. When ν(CO)$_{ads}$ data (obtained from spectra of the Rh sol/CO system acquired with time) is plotted vs observed absorbance, the graph exhibits positive slope for most of the data, thus supporting this suggestion.

In contrast, ν(CO)$_{ads}$ for the B_2 mode of adsorbed CO appears to vary by only ±3 cm^{-1} with time. However, this broad, usually weak band is difficult to monitor in infrared spectra because of residual baseline effects after subtraction of the water spectrum. The invariance of the ν(CO)$_{ads}$ band due to bridged CO could indicate island formation of adsorbed CO as was suggested for CO adsorbed[4] on palladium hydrosols.

(iv) Adjusted pH Studies. Figure 6 represents a series of infrared spectra of the Rh sol/CO system at various adjusted pH values. Figure 7 is a plot of ν(CO)$_{ads}$ vs pH for CO adsorbed linearly on a rhodium hydrosol. In general, the PVA-protected rhodium hydrosol possessed similar stability to the PVA-protected platinum hydrosol since no aggregation of the hydrosol occurred over the pH range 0–12. Above the natural pH of ca. 2.2, ν(CO)$_{ads}$ decreases steadily with increasing pH from a maximum value of ca. 2047 to 2000 cm^{-1}. CO coverage as estimated from the normalized absorbance[4] (A′(CO)) of the ν(CO)$_{ads}$ band is also observed to decrease as the pH of the dispersion medium is increased. It is evident that the influence of

(28) Mucalo, M. R.; Cooney, R. P., submitted to *J. Colloid Interface Sci.*

(29) Nichols, H.; Hexter, R. M. *J. Chem. Phys.* **1980**, *73*, 965.

pH on CO adsorption on rhodium hydrosols is similar to that observed for CO adsorption on platinum hydrosols.[4] Thus as pH increases and in the presence of atmospheric oxygen, it is expected that growth of rhodium oxides (e.g., Rh_2O_3) on the surface of the hydrosol particles (as predicted[30] from the Pourbaix diagram of the Rh–H_2O system) will lead to effective blocking of CO adsorption sites and hence a decrease in CO coverage. Indeed, hydrated rhodium sesquioxide ($Rh_2O_3 \cdot 5H_2O$) is known[31] to form from addition of base to Rh(III) solutions. Therefore, $\nu(CO)_{ads}$ decreases as a result of reduced dipolar coupling between adsorbed CO molecules on the rhodium surface.[4]

For pH below the natural pH (i.e., in the pH range 0–2), CO adsorption on rhodium hydrosols is slightly enhanced. This enhancement is inferred from $\nu(CO)_{ads}$–A′(CO) (normalized absorbance) correlations, which have showed similar behavior when CO adsorption[6] on Pt(PVA) hydrosols below the natural pH of ca. 4.0 was studied. However, enhancement of CO adsorption on PVA-protected rhodium hydrosols at pH < natural pH (ca. 2.2) occurs to a lesser extent than for PVA-protected platinum hydrosols at pH < natural pH (ca. 4.0; see ref 6). Enhancement in CO adsorption as pH is decreased below 2.0 may arise from partial detachment of adsorbed poly(vinyl alcohol) induced by acid-catalyzed transformations of poly(vinyl alcohol) molecules, which is inferred[6] to be responsible for enhanced CO adsorption on PVA-protected platinum hydrosols in acidic media. At very low pH, $\nu(CO)_{ads}$ appears to plateau at 2045–2047 cm^{-1} (Figure 7). This may arise from the presence of coadsorbed poly(vinyl alcohol), which could induce the growth of CO islands on the rhodium hydrosol particles.

In general, $\nu(CO)_{ads}$ for the band due to bridge-adsorbed (B_2) CO on rhodium metal appears to be invariant with pH until very high pH where it has been observed in spectra as a weak feature at a reduced frequency of ca. 1870 cm^{-1}. The spectroscopic behavior of the bridging carbonyl band in spectra of CO-treated rhodium hydrosol is reminiscent of that exhibited[4] by the $\nu(CO)_{ads}$ band for bridge-adsorbed CO on palladium hydrosols. Therefore, the invariance in pH could be ascribed to island formation of bridged CO as suggested[4] in the Pd sol/CO system. Sharp decreases in $\nu(CO)_{ads}$ at high pH could be attributed to pronounced changes in rhodium surface characteristics arising probably from the competitive adsorption of hydroxide to form rhodium oxides.

(v) Comparison with the Electrode/Electrolyte Interface. Comparisons with CO adsorption at the electrode/electrolyte interface will be made for the Rh sol(PVA)/CO system by using frequency–pH data from the adjusted pH studies using a procedure identical to that used for the analysis of data arising from infrared studies of CO adsorption on protected[6] and unprotected[4] platinum hydrosols as a function of pH.

It has been demonstrated[6] for PVA-protected platinum hydrosols that the protecting agent has a noticeable effect on $\nu(CO)_{ads}$. However, the decrease of $\nu(CO)_{ads}$ with increasing pH is still an important feature of studies relating to CO adsorption as a function of pH on protected platinum hydrosols. Therefore, interpretations from the comparative study of rhodium hydrosol/electrode surface chemistry should also take account of the influence of the poly(vinyl alcohol) on surface chemistry. Earlier, it was shown that X-ray photoelectron spectra of the unprotected rhodium hydrosol suggested the presence of surface Rh_2O_3. By inference, the PVA-protected hydrosol particles are also assumed to possess a thin oxide surface layer. The model as applied to platinum and palladium hydrosols[4] considers the hydrogen ion to be[32] a primary surface potential determining ion in the thin oxide layer on the hydrosol particles. The equations outlined in ref 4 are then assumed to apply, which lead to the following:

$$\frac{d\nu}{d\psi_0} = \frac{(-d\nu/d(pH))F}{2.303RT} \quad (1)$$

In eq 1, ψ_0 is defined as surface potential on the hydrosol particles and ν refers to $\nu(CO)_{ads}$. Table I gives a summary of the results obtained in the calculation of $d\nu/d\psi_0$ from $d\nu/d(pH)$ (from Figure 7) for the Rh sol/CO system. In the pH range 0–2, $d\nu/d\psi_0$ occurs in the range 26–40 cm^{-1} V^{-1}. This is comparable to $d\nu/dE$ values obtained for CO adsorbed[13] on polycrystalline rhodium electrodes in 0.5 M H_2SO_4 (40 cm^{-1} V^{-1}) and for CO adsorbed[13] on single Rh(111) crystals in 0.1 M $HClO_4$ (35 cm^{-1} V^{-1}). Thus, CO adsorbed on protected rhodium hydrosols appears to exhibit a behavior similar to that of CO adsorbed on single-crystal and polycrystalline electrodes. In comparison, CO adsorbed on (aggregated) unprotected platinum hydrosol particles did not behave[4] as CO adsorbed at a polycrystalline electrode in acidic media since $d\nu/d\psi_0$ was calculated to be ca. −40 cm^{-1} V^{-1} at pH 3.37. However, aggregation of rhodium hydrosols at low pH is prevented only by the adsorbed poly(vinyl alcohol) protecting agent. Thus, the importance of the poly(vinyl alcohol) at pH below the natural pH of ca. 2.2 in contributing to the apparently close correspondence of colloid and electrode surface chemistry in rhodium hydrosols is evident. According to Table I, $d\nu/d\psi_0$ increases as the pH of the rhodium hydrosol dispersion medium increases. This phenomenon was also observed in previous infrared studies[4] of CO adsorption on unprotected platinum hydrosols as a function of pH, although the increase in $d\nu/d\psi_0$ for the Pt sol/CO system was more pronounced in the pH range 10–12. Thus, the decline in $\nu(CO)_{ads}$ as pH of the rhodium hydrosol is increased may be considered to be a consequence of an increase in the $d_\pi(Rh)$–$\pi^*(CO)$ bonding due to the increase in negative surface charge resulting from hydroxide adsorption. Earlier studies[4] of CO adsorption on platinum hydrosols as a function of pH have claimed that increases in $d\nu/d\psi_0$ with pH reflect competition of OH^- (as surface oxide growth increases with increasing pH) with CO adsorption sites on the platinum

Table I. Calculated Values of $d\nu/d\psi_0$ from $d\nu/d(pH)$ for the Rh sol(PVA)/CO Adjusted pH Experiments

pH	$\nu(CO)_{ads}$,[a] cm^{-1}	$d\nu/d(pH)$, cm^{-1}	$d\nu/d\psi_0$, cm^{-1} V^{-1}
0.30	2045.0	−1.53	26.3
0.60	2044.5	−1.65	28.4
1.0	2043.8	−1.82	31.3
2.0	2041.8	−2.24	38.5
4.0	2036.4	−3.08	53.0
6.0	2029.4	−3.92	67.4
8.0	2020.8	−4.76	81.9
10.0	2010.4	−5.60	96.3
11.0	2004.6	−6.02	103.5
12.0	1998.4	−6.44	110.8

[a] This frequency was calculated from the equation of the fitted x^2 polynomial to the $\nu(CO)_{ads}$ vs pH curve for the Rh sol/CO system (Figure 7) at the pH stated.

(30) Llopis, J. F.; Tordesillas, I. M.; Colom, F. *Encyclopaedia of Electrochemistry of the Elements*; Bard, A. J., Ed.; Marcel Dekker: New York, 1976; Vol VI, p 171.

(31) Bailar, J. C.; Emeleus, H. J.; Nyholm, R.; Trotman-Dickenson, A. F. *Comprehensive Inorganic Chemistry*; Pergamon Press: Oxford, 1973; p 1236.

(32) Furlong, D. N.; Launikonis, A.; Sasse, W.H.F. *J. Chem. Soc., Faraday Trans. 1* **1984**, *80*, 571.

hydrosol particles. With similar decreases in $\nu(CO)_{ads}$ at basic pH and large increases in $d\nu/d\psi_0$ at high pH (see Table I), it appears that such competition for CO adsorption sites may also operate in the PVA-protected Rh sol/CO system.

Acknowledgment. We express our gratitude toward the New Zealand University Grants Committee for the provision of funds to purchase the Fourier transform infrared spectrometer and for the awarding of a Postgraduate and William Georgetti scholarship to M.R.M.

Registry No. CO, 630-08-0; Rh, 7440-16-6; poly(vinyl alcohol), 9002-89-5.

Selective Leaching of Copper and Barium from the $YBa_2Cu_3O_{7-x}$ Superconductor by Chelating Diamines

Patrick M. James, Eric J. Thompson, and Arthur B. Ellis*

Department of Chemistry, University of Wisconsin—Madison, Madison, Wisconsin 53706

Received June 6, 1991. Revised Manuscript Received September 4, 1991

Rapid selective leaching of Cu and Ba from the superconductor $YBa_2Cu_3O_{7-x}$ (1–2–3) is effected by exposure of the solid to aqueous and mixed H_2O/MeOH solutions of ethylenediamine (en). Inductively coupled plasma emission spectroscopy revealed that virtually all of the Cu and most of the Ba are in the solution phase; almost all of the Y is in the solid residue resulting from the reaction. X-ray diffraction analysis and IR spectroscopy are consistent with the solid product being primarily amorphous $Y(OH)_3$. The solid also contains small quantities of $BaCO_3$ and Y_2BaCuO_5(2–1–1); the $BaCO_3$ is formed by reaction of Ba^{2+} ions in the leaching solution with CO_2, while the 2–1–1 was initially present as an impurity in the 1–2–3 samples employed and is comparatively unreactive toward the leachant. The leaching process was monitored spectrophotometrically through the formation of the purple *trans*-diaquobis(ethylenediamine)copper(II) complex. Kinetic studies reveal that the initial reaction rate is directly proportional to the 1–2–3 macroscopic apparent surface area. In mixed H_2O/MeOH solutions the leaching rate follows a first-order rate law with the concentrations of water (2.5–30 M range in 2.0 M en) and ethylenediamine (0.12–2.5 M range in 30 M water). Concentrated en solutions gave corrosion rates of up to ~0.2 μm/min at room temperature, with rates increasing to ~1 μm/min at 65 °C. The temperature dependence of the reaction rate yields an apparent activation energy of 55 ± 5 kJ/mol between 25 and 65 °C. Substitution of D_2O for H_2O in the leachant solution roughly halves the reaction rate at room temperature. Chelation appears to supply a significant driving force for the reaction: 1,2-diaminopropane, 1,3-diaminopropane, *sym*-dimethylenediamine, triethylenediamine, and 2,2′-bipyridine also serve as leachants. The leaching rate is negligible at room temperature with a variety of monoamines and nonchelating diamines.

Introduction

Despite the enormous interest in the superconductor $YBa_2Cu_3O_{7-x}$ (1–2–3), there have been few systematic studies of the reactivity of this compound under ambient conditions. The electrochemical behavior of 1–2–3 in various aqueous media has been investigated.[1,2] Also, aqueous solutions of EDTA have been used to decompose 1–2–3, presumably by chelating the constituent cations, and can etch micropatterns into the solid.[3] Among the reactions that have been characterized are those with water and CO_2, which lead to nonsuperconducting products.[4–9] Yan et al. have proposed that the reaction with water proceeds by

$$2YBa_2Cu_3O_7 + 3H_2O \rightarrow Y_2BaCuO_5 + 3Ba(OH)_2 + 5CuO + \tfrac{1}{2}O_2 \quad (1)$$

with the $Ba(OH)_2$ undergoing further reaction with CO_2 to yield $BaCO_3$:

$$Ba(OH)_2 + CO_2 \rightarrow BaCO_3 + H_2O \quad (2)$$

In this paper we provide evidence that chelation by aqueous and mixed H_2O/MeOH ethylenediamine (en) solutions can rapidly and selectively solubilize Cu and Ba cations from the 1–2–3 lattice at room temperature, resulting in a Y-rich, insulating solid residue. The reaction, which can be monitored spectrophotometrically, has been measured to proceed at a rate of up to ~0.2 μm/min at room temperature. We demonstrate herein that the reactivity depends strongly on solvent, temperature, and amine, permitting the rate to be tuned over several orders of magnitude. The ability to control etching rate in this manner may be useful in device fabrication schemes employing 1–2–3.

Experimental Section

Materials. Unless otherwise specified, all experiments involving 1–2–3 were conducted with powder or sintered pellets obtained from HiT$_c$ Superconco, Inc., Lambertville, NJ, that contained nearly exclusively single-phase 1–2–3 as shown by X-ray powder diffraction. Additional sample details were provided by

(1) Rosamilia, J. M.; Miller, B.; Schneemeyer, L. F.; Waszczak, J. V.; O'Bryan, Jr., H. M. *J. Electrochem. Soc.* **1987**, *134*, 1863.
(2) Magee, V. M.; Rosamilia, J. M.; Kometani, T. Y.; Schneemeyer, L. F.; Waszczak, J. V.; Miller, B. *J. Electrochem. Soc.* **1988**, *135*, 3026.
(3) Shokoohi, F. K.; Schiavone, L. M.; Rogers, C. T.; Inam, A.; Wu, X. D.; Nazar, L; Venkatesan, T. *Appl. Phys. Lett* **1989**, *55*, 2661.
(4) Barns, R. L.; Laudise, R. A. *Appl. Phys. Lett.* **1987**, *51*, 1373.
(5) Yan, M. F.; Barns, R. L.; O'Bryan, H. M. Jr.; Gallagher, R. C.; Sherwood, R. C.; Jin, S. *Appl. Phys. Lett.* **1987**, *51*, 532.
(6) Nakada, I.; Sato, S.; Oda, Y. *Jpn. J. Appl. Phys.* **1987**, *26*, L697.
(7) Narottam, P.; Sandkuhl, B.; Sandkuhl, A. L. *Appl. Phys. Lett.* **1988**, *52*, 323.
(8) Veretnik, D.; Reich, S. *Appl. Phys. Lett.* **1990**, *56*, 2150.
(9) Tressaud, A.; Amine, K.; Chaminade, J. P.; Etourneua, J. *J. Appl. Phys.* **1990**, *68*, 248.

0897-4756/91/2803-1087$02.50/0